


Exciton Delocalization in Amino-Functionalized Inorganic MoS₂ Quantum Disks: Giant Davydov Splitting and Exchange Narrowing

Denice N. Feria,¹ Wei-Jie Jhan,¹ Yu-Ting Chen,¹ Hong-Jyun Wang¹,¹ Svette Reina Merden Santiago,¹ Chi-Tsu Yuan,¹ Chih-Lung Chou,¹ Ji-Lin Shen^{1,*},¹ Tai-Yuan Lin,² Guan-Zhang Lu,³ and Yang-Fang Chen^{3,†}

¹*Department of Physics and Center for Nanotechnology, Chung Yuan Christian University, Chung-Li 320314, Taiwan*

²*Department of Optoelectronics and Materials Technology, National Taiwan Ocean University, Keelung 202, Taiwan*

³*Department of Physics, National Taiwan University, Taipei 10617, Taiwan*

 (Received 22 June 2020; revised 16 November 2020; accepted 7 January 2021; published 4 February 2021)

Exciton delocalization, a phenomenon in which spatial extension of the excitons spreads over aggregates, has attracted significant attention in both academia and industry. Studies on exciton delocalization focus mainly on dye molecules and organic conjugated solids because of their high binding energies. Here, we report on exciton delocalization from inorganic MoS₂ quantum disks (QDs) functionalized with diethylenetriamine (DETA). By increasing the QD concentration, a giant Davydov splitting with an energy of up to 850 meV and an exchange narrowing with an exciton delocalization length up to several tens of QDs are observed. Notably, exciton delocalization in amino-functionalized MoS₂ QDs can be controlled by the DETA concentration. Amino-related bonding is suggested to modulate the Davydov splitting. Understanding the mechanism of exciton delocalization in two-dimensional QDs is expected to be useful and open up a route for the discovery of unique physical phenomena and the development of as-yet unrealized devices.

DOI: [10.1103/PhysRevApplied.15.024011](https://doi.org/10.1103/PhysRevApplied.15.024011)

I. INTRODUCTION

Exciton delocalization, a phenomenon by which delocalized electronic excited states are distributed over spatially separated molecular aggregates, has attracted considerable attention because of its fundamental interest and potential applications [1–4]. Extension of the delocalized excited states in molecular aggregates due to intermolecular coupling can be described as a coherent linear superposition of quantum-mechanical wave functions in isolated molecules [5]. Thus, excitation occurs in a quantum superposition of different molecular exciton states, leading to electronic coherence in molecular aggregates. The exciton delocalization found in molecular aggregates offers a noticeable impact on the electronic and optical properties, which is different from those in isolated molecules. For instance, a splitting of exciton states, known as Davydov splitting, originates from the overlap of the delocalized wave function. This mechanism is exhibited in absorption spectra [6–8]. The magnitude of Davydov splitting depends on the intermolecular strength of the interaction and the relative orientation in molecular

aggregates. Also, strong intermolecular interactions reduce the effect of homogenous spectral broadening. This reduction leads to an exchange narrowing of the exciton band, which is attributed to the dynamic average of inhomogeneous broadening in exciton bands [9,10]. Accordingly, the absorption peak in coupled molecular aggregates is considerably narrower than that in the isolated molecules. Exchange narrowing may occur in paramagnetic resonance, J-band molecular aggregates, and other excitonic transitions [9]. Other exciton delocalization effects, such as J- or H- aggregate behavior and super-radiance are also observed in molecular aggregates by absorption or photoluminescence (PL) spectroscopies [11–17].

In inorganic semiconductors, some signatures of exciton localization-delocalization are observed through the Stokes shift or the temperature dependence of PL studies [18–20]. However, no further investigations on Davydov splitting and exchange narrowing have been reported for these materials. Recently, two-dimensional (2D) semiconductors have attracted much attention, owing to their peculiar physical properties and potential applications. Because of their relatively heavy effective masses and reduced dielectric screening, monolayered 2D semiconductors build firmly bound excitons with binding energies of hundreds of meV [21], making them suitable for

*jlshen@cycu.edu.tw

†yfchen@phys.ntu.edu.tw

investigating Davydov splitting. Furthermore, an exciton binding energy as high as about 1 eV can be produced when the lateral dimension of these 2D semiconductors is reduced to the nanoscale or synthesized as quantum disks (QDs) [22]. In this manner, excitons are strongly localized in QDs. When the QDs form a thin film, the aggregated QDs can induce a strong coupling between localized excitons in individual QDs and lead to exciton delocalization. Therefore, 2D QDs provide an excellent platform to study intriguing Davydov splitting and exchange narrowing.

In this study, we introduce an approach to alter inter-disk coupling by adjusting the concentration of amine-functionalized MoS₂ QDs. Davydov splitting from the amino-functionalized MoS₂ QD aggregates is observed using photoluminescence excitation (PLE) and absorption spectroscopies, demonstrating the exciton delocalization effect in 2D transition-metal dichalcogenides (TMDs). The energy of Davydov splitting can be easily controlled by tuning the concentration of the amino-functionalized MoS₂ QD solution (dilution) without requiring any other chemical modification. With an increase in QD concentration, a reduction of the line width in the PLE peak is also observed, which reveals a strong exchange narrowing in the exciton transition spectra. The Davydov splitting can be as large as 850 meV, and the exchange narrowing can reach an exciton delocalization length of up to several tens of QDs. Furthermore, the effect of the diethylenetriamine (DETA) concentration on interdisk coupling in MoS₂ QD aggregates is analyzed. An understanding of exciton delocalization in 2D QDs is useful for practical applications in optoelectronic devices [23–26]. For example, modulation of the exciton absorption in MoS₂ QDs is advantageous for making saturable absorbers, which is essential for generating ultrafast mode-locked laser pulses [25]. Also, the tunability of exciton response in MoS₂ QDs is beneficial for generating four-wave mixing processes, which can be applied to frequency conversion, imaging, and optical signal amplification [26].

II. EXPERIMENT

The DETA-functionalized MoS₂ solution is prepared by dispersing 0.015 g of MoS₂ ultrafine flakes (Graphene Supermarket) in 7 ml ethanol. Different molar concentrations of DETA from 0.015 to 1.543M (Sigma Aldrich, 99%) are added to the prepared solution for the functionalization of MoS₂ QDs. After that, the mixture is ultrasonicated for 30 min. A top-down process, namely, the pulsed laser ablation (PLA) method, is used to synthesize the MoS₂ QDs. In this process, an optical parametric oscillator (OPO) laser with a repetition rate of 10 Hz and fluence of 2.58 J/cm² is used to ablate the DETA-functionalized MoS₂ precursor solution. The utilized pulsed laser is set at an excitation wavelength of 415 nm and the synthesis is set to 30 min during which time the sample is

concurrently mixed on a rotator stage at 80 rpm. The samples are centrifuged for 2 h and filtered to become amino-functionalized MoS₂ QDs. The QD concentration is estimated according to the volume of a QD and the density of MoS₂ [27].

The structural properties of DETA-functionalized MoS₂ QDs are observed using transmission electron microscopy (TEM) on a JEOL JEM-2100F system with an operating voltage of 200 kV. Additionally, x-ray photoelectron spectroscopy (XPS) on a Thermo Scientific K-Alpha ESCA instrument, equipped with a monochromatic Al K α x-ray source at 1486.6 eV, is carried out to analyze the chemical-bonding components of DETA-functionalized MoS₂ QDs. Ultraviolet-visible spectroscopy (UV-vis) is evaluated using a Jasco V-750 spectrophotometer [using a photomultiplier tube (PMT) with spectral resolution of approximately 0.5 nm]. PL and PLE are measured using a FluoroMax-4 spectrofluorometer (Horiba Scientific) with emission bandwidths of 2 and 3 nm, respectively, resulting in a spectral resolution of about 0.5 nm. The PL and PLE measurements are carried out with a 0.2 \times 1 cm² quartz cuvette using a 150-W ozone-free xenon lamp with a power density of 2.5 mW/cm² as the excitation source. The excitation (emission) wavelength is set at 360 nm (450 nm) for PL (PLE) measurements. The luminescence is collected through a grating (1200 gr/mm blazed at 500 nm) with a 90° geometry and detected with an R928P PMT with an integration time of 1 s. All of the optical measurements are carried out at 300 K.

III. RESULTS AND DISCUSSION

Figure 1(a) shows the TEM image of QDs synthesized after pulsed laser ablation, indicating a monodisperse distribution. The high-resolution (HR) TEM image shown in Fig. 1(b) reveals that the MoS₂ QDs have a lattice spacing of about 0.27 nm, which corresponds to the interplanar distance of d_{100} in MoS₂ [28]. Figure 1(c) displays the results of the statistical analysis of the TEM images, which gives a Gaussian distribution with an average size of about 4.5 nm. Based on atomic force microscopy (AFM) measurements (not shown), the thickness of the MoS₂ QDs is found to be about 4.5 nm. This thickness corresponds to about seven monolayers of MoS₂, since the thickness of a monolayer is about 0.65 nm, including a three-atom-thick S-Mo-S layer (thickness = 0.301 nm) and a van der Waals gap (thickness = 0.314 nm) [29].

The Mo region of XPS is investigated and displayed in Fig. 2(a). The binding energies at about 228, 231, and 235 eV correspond to Mo⁴⁺ 3d_{5/2}, Mo⁴⁺ 3d_{3/2}, and Mo⁶⁺ 3d_{3/2}, respectively [30]. On the other hand, Fig. 2(b) demonstrates the S region of XPS, revealing binding energies at 162, 163, and 168 eV, corresponding to S²⁻ 2p_{3/2}, S²⁻ 2p_{1/2}, and S⁴⁺ peaks, respectively [31]. Also, DETA is found to be attached to the MoS₂ QDs due to the

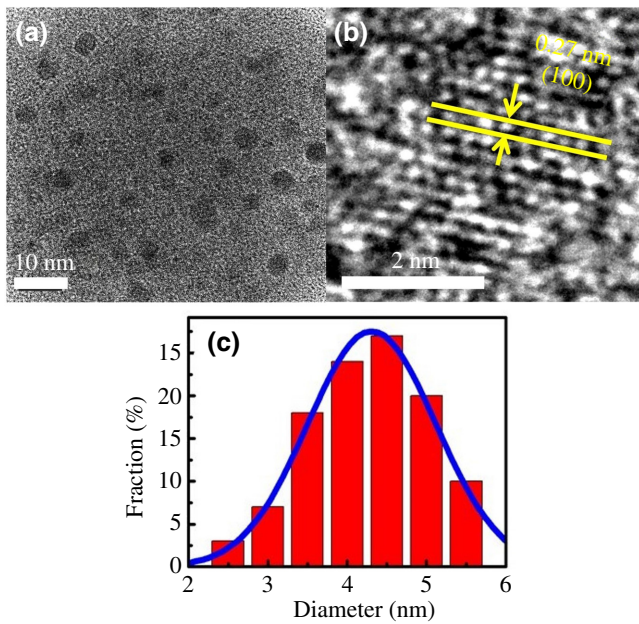


FIG. 1. (a) TEM image, (b) HRTEM image, and (c) size distribution of amino-functionalized MoS_2 QDs.

peak present that is attributed to the N—Mo bond at about 399 eV, as shown in Fig. 2(c) [32]. Figure 3 shows that the MoS_2 QDs synthesized with different concentrations of DETA reveal blue luminescence under UV light with a power density of $720 \mu\text{W}/\text{cm}^2$. This reflects that the use of pulsed laser ablation in producing the DETA-functionalized MoS_2 QDs is successful.

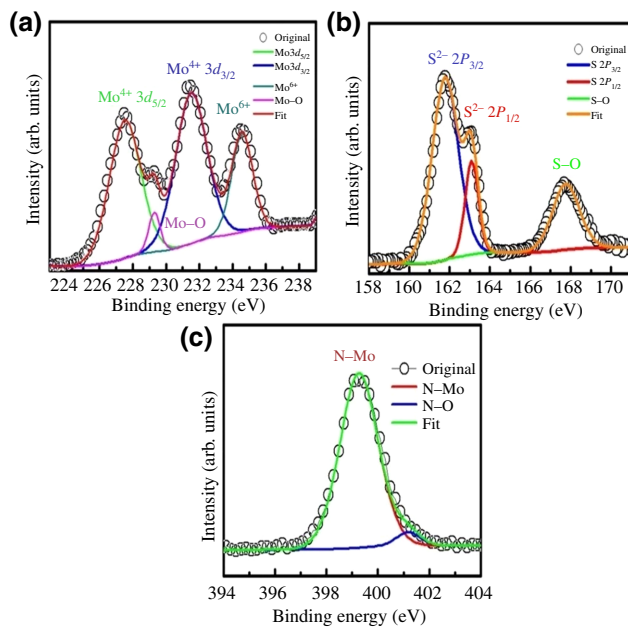


FIG. 2. (a) Mo 3d, (b) S 2p, and (c) N-Mo XPS spectra of amino-functionalized MoS_2 QDs.

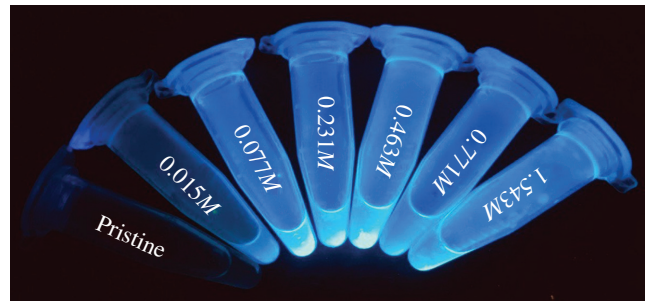


FIG. 3. Optical photographs of different amino-functionalized MoS_2 QDs under UV light [DETA concentration changes from 0 to 1.543M (left to right)].

To observe exciton delocalization, it is essential to control the intermolecular distance in aggregates. One way to adjust the distance between QDs is to change the QD concentration [33]. With an increase in QD concentration, the average distance between neighboring QDs decreases. This could modify the exciton coupling between QDs. Figure 4 shows the optical absorption spectrum of amine-functionalized MoS_2 QDs at various QD concentrations. The optical absorption spectrum exhibits an absorption peak near 3.45 eV and a steplike absorption band near 4.25 eV, which can be assigned as the *A*-exciton peak and quasiparticle continuum states, respectively [21,22]. As the QD concentration increases, the absorption peak at about 3.4 eV broadens and a plateaulike region is formed for QD concentrations of 5.9 and $8.9 \mu\text{M}$. The absorption peaks observed consist of several unresolved components.

Traditionally, absorption spectroscopy is a convenient and sensitive technique to determine the exciton absorption in luminophores. An alternative way to provide information on the exciton absorption is through PLE spectroscopy. Figure 5(a) describes the PL, PLE, and absorption spectra of amino-functionalized MoS_2 QDs

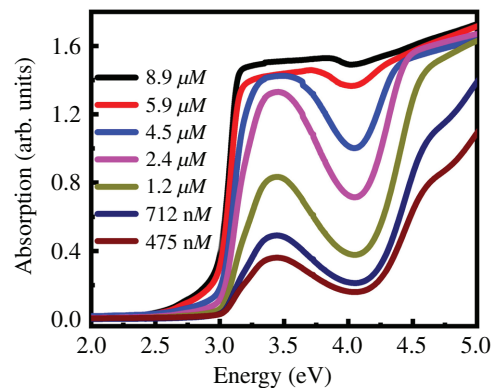


FIG. 4. Optical absorption spectra of amino-functionalized MoS_2 QDs [DETA concentration = 0.463M] in different QD concentrations.

with a QD concentration of 475 nM. The PL, which is indicated by the solid line, displays two main peaks around 2.7 and 2.8 eV, which are attributed to excitons bound to different defects and/or surface states (DX states) [22]. The corresponding PL spectra of amine-functionalized MoS₂ QDs with different QD concentrations are shown in Fig. 5(b). These results show that the PL intensity of MoS₂ QDs decreases with increasing QD concentrations. The decrease in PL intensity could be due to the exciton delocalization process (exciton coupling) between nearest-neighbor QDs [34]. However, the PL peak positions remain unchanged. On the other hand, the PLE spectrum of the amine-functionalized MoS₂ QDs is described by monitoring the emission energy at 2.75 eV. This reveals a main peak at about 3.4 eV and a small peak at about 4.55 eV. The absorption spectrum of the same sample is also displayed in Fig. 5(a) for comparison. The peaks at 3.4 and 4.55 eV in the PLE spectra match the *A*-exciton peak and quasiparticle continuum states in the absorption spectrum, respectively. Because of this, PLE is an alternative tool that can be used to investigate the exciton transition in MoS₂ QDs.

Figure 6(a) displays the PLE spectra of amine-functionalized MoS₂ QDs at different QD concentrations. The PLE peak observed at 3.4 eV is independent of the QD concentration of 712 nM. However, beyond a QD concentration of 712 nM, the broad exciton peak at 3.4 eV begins to split into two components: a redshifted intense peak and the other blueshifted weak peak. Splitting of the exciton peak becomes increasingly pronounced during an increase in the QD concentration. The two split peaks are observed above a concentration of 1.2 μM. Using Gaussian functions, the PLE spectrum of amine-functionalized MoS₂ QDs can be fitted with two peaks, as shown in Fig. 6(b). Compared with the absorption spectra (Fig. 4), the PLE spectra reveal much better resolution, while detecting the exciton peak splitting. Figure 6(c) shows the energies of the exciton peaks as a function of QD concentrations, which indicate an increase in energy splitting together with the QD concentration. An energy splitting as high as 850 meV is achieved at a QD concentration of 8.9 μM, as shown in Fig. 6(d). This energy splitting (Davydov splitting) not only demonstrates exciton delocalization in the amino-functionalized MoS₂ QDs due to exciton coupling between QDs, but also proves that the PLE technique is a very powerful tool to detect excitons in the QD aggregates. The Davydov splitting mechanism observed in the PLE spectra is more pronounced than that of the absorption spectra due to the many transitions involved in the absorption processes, which are not able to generate radiative recombination. Therefore, the absorption spectra are broader than the PLE spectra, which cannot be used to distinguish the Davydov splitting.

The Davydov splitting of the absorption band in PLE can be ascribed to exciton-exciton coupling between

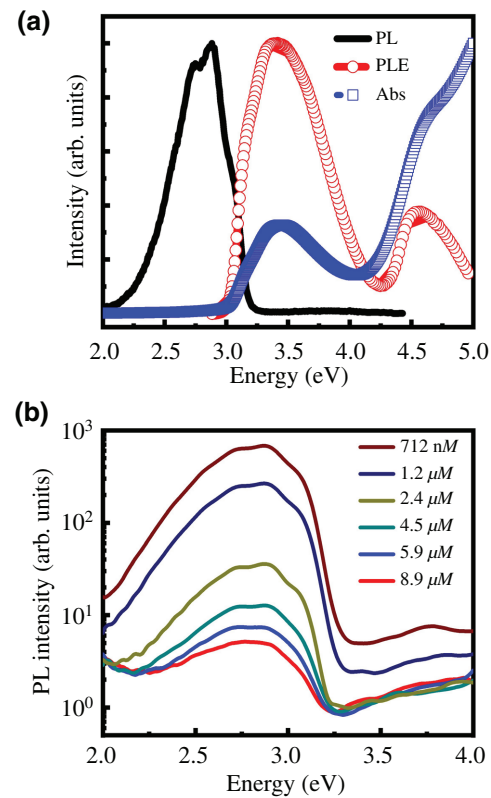


FIG. 5. (a) Optical absorption, PL, and PLE spectra of amino-functionalized MoS₂ QDs at a QD concentration of 475 nM. Excitation (emission) wavelength is set at 360 nm (450 nm) for PL (PLE) measurements using an ozone-free xenon lamp with a power density of 2.5 mW/cm². All of the optical measurements are carried out using a PMT detector and performed at 300 K. (b) PL of amine-functionalized MoS₂ QDs at different QD concentrations (DETA concentration = 0.463 M).

nearest-neighbor QDs in close-packed proximity. This splitting of excitons is generally attributed to the dipole-dipole interaction between two luminophores [35]. Most of the Davydov splitting due to exciton delocalization is reported in organic materials, such as dye molecules and conjugated solids [16,35]. Here, we demonstrate giant Davydov splitting in an inorganic semiconductor system. This giant Davydov splitting can be attributed to the results arising from the large exciton binding energy (approximately hundreds of meV), which allows the existence of an exciton at room temperature. In Fig. 6(a), the intensity of the redshifted peak is much larger than that of the blueshifted peak, indicating that the interdisk coupling in our system is mostly of J-type aggregate behavior [36]. Figure 6(d) shows the energy splitting of excitons in the amino-functionalized MoS₂ QDs as a function of the QD concentration. The splitting magnitude is evidently enhanced as the QD concentration increases from 0.36 to 2.97 μM, but it saturates gradually as the concentration exceeds 3.6 μM. Thus, the energy splitting, $\Delta\varepsilon$, can be

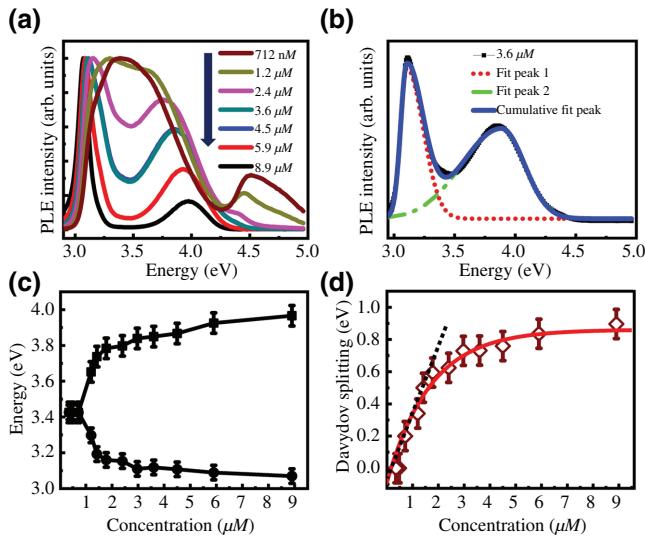


FIG. 6. (a) PLE spectra of amino-functionalized MoS_2 QDs for different QD concentrations with DETA concentration = $0.463M$. (b) Example of Gaussian fitting used for the analysis of PLE peaks. (c) Energy position of PLE peaks (lines are guides to the eye and black data points are peaks of the splitting). (d) Energy splitting of the exciton peak for different QD concentrations. Dashed line displays fitted linear curves from Eq. (2), while solid line demonstrates fitted curves based on Eq. (3) with $r_{\min} = 1.05$ nm and $\alpha = 0.60 \mu\text{M}^{-1}$.

analyzed based on a molecular exciton model [35,37,38]:

$$\Delta\varepsilon \propto r^{-3}, \quad (1)$$

where r is the distance to the nearest neighbor. Assuming that the QDs are expanded in a uniform cubic lattice and the number of nearest neighbors remains constant, r can be associated with the QD concentration, C , through $r \propto C^{-1/3}$ [39]. Then, the value of $\Delta\varepsilon$ can be related to C through the following relation:

$$\Delta\varepsilon \propto C. \quad (2)$$

The dashed line in Fig. 6(d) displays the linear curve fitted using Eq. (2). The experimental Davydov splitting with increasing C from 0.36 to $2.97 \mu\text{M}$ agrees well with the above relation. However, after C exceeds $2.97 \mu\text{M}$, the Davydov splitting converges toward its saturation value. Intuitively, one should not expect that the Davydov splitting will continuously increase directly with C without limitation. Hence, there exists a shortest distance of QD nearest neighbors, r_{\min} , which could be due to blockage of the surface functional groups or the repulsive force in-between the QDs when they are very close to each other. Indeed, saturation of the Davydov splitting for a large number of organic conjugated chains has also been reported in previous studies [17].

To describe the abovementioned saturated effect of Davydov splitting, a simple physical model is used to construct exciton coupling for different QD concentrations. In a molecule-coupling system, the coupling strength can be related to the number of (coupled) nearest neighbors [38]. We suggest that the coupling strength at high C will decay with C because r cannot decrease without limitation. By assuming that the decay rate of the coupled QD number, N , in a given C ($-dN/dC$) is proportional to the number of existing coupled QDs (N), this leads to a relation of $-dN/dC = \alpha N$, where α is a proportionality parameter. After integration, the coupling strength (N) to C is represented by $e^{-\alpha C}$. According to this underlying mechanism, we propose a new empirical formula based on Eq. (1) and consider the saturated coupling effect ($e^{-\alpha C}$) to meet the realistic Davydov splitting as a function of C :

$$\Delta\varepsilon \propto r_{\min}^{-3}(1 - e^{-\alpha C}), \quad (3)$$

where r_{\min} is the minimum distance of the nearest-neighbor QD and α is a parameter to modify the decay of exciton coupling. Using Eq. (3), with $r_{\min} = 1.05$ nm and $\alpha = 0.60 \mu\text{M}^{-1}$, the energy splitting is displayed as a solid line in Fig. 6(d). When C is small, the value of $e^{-\alpha C}$ is about $1 - \alpha C$ and $\Delta\varepsilon$ corresponds to the result from Eq. (1). On the other hand, when C is large, the value of $e^{-\alpha C}$ is about zero and $\Delta\varepsilon$ approaches a constant. Thus, Eq. (3) reproduces the equation of Davydov splitting as a function of C quite well.

In Fig. 7(a), the line width of the split redshifted peak (~ 3.1 eV) is reduced with increasing QD concentration. The reduction in the exciton line width is also an effect of exciton delocalization because of strong coupling between QD aggregates. The coupled exciton delocalizes over many sites of QDs and induces an average inhomogeneous broadening, leading to the so-called exchange narrowing [10]. According to the model of spatially uncorrelated Gaussian diagonal disorder, exchange narrowing reveals a $C^{-1/2}$ dependence of the line width in an absorption band

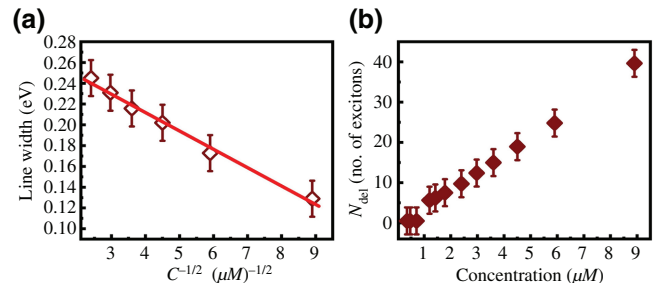


FIG. 7. (a) Line-width narrowing measurements as a function of $C^{-1/2}$. Values are extracted from the FWHM of the redshifted peak found in Fig. 6(a) of amino-functionalized MoS_2 QDs. (b) Exciton delocalization length as a function of QD concentration (DETA concentration = $0.463M$).

[9]. Upon measuring the narrowing in terms of line width, the full width at half maximum (FWHM) is obtained from the PLE measurements. Thus, we plot the $C^{-1/2}$ dependence of the FWHM of the redshifted peak (~ 3.1 eV) extracted from Fig. 6(a), as shown in Fig. 7(a). The measured FWHM agrees well with the linear dependence of $C^{-1/2}$, proving exchange narrowing and exciton delocalization in the amino-functionalized MoS₂ QDs. After that, we can estimate the exciton delocalization length (i.e., the number of molecules over which the exciton is coherently delocalized) from the exciton line width. The exciton delocalization length is associated with competition between exciton coupling and environmental static disorder [40]. According to the line width of the J band, the exciton delocalization length is approximated using [41]

$$N_{\text{del}} = \frac{3}{2} \left(\frac{\Delta v_{\text{mon}}}{\Delta v_J} \right)^2 - 1, \quad (4)$$

where Δv_{mon} is the line width (FWHM) of the monomer of the absorption band and Δv_J is the line width of the J band. By extracting the FWHM from Fig. 6(a), the values of N_{del} in the amino-functionalized MoS₂ QDs as a function of QD concentration are obtained, as displayed in Fig. 7(b). The calculated value of N_{del} is found to be proportional to the QD concentrations. This indicates that more QDs may provide more opportunity for a QD to couple with others, causing the coupled exciton to extend over more sites in the QD aggregates. N_{del} attains the highest value of 39 QDs, which reveals a high degree of ordering of aggregates at room temperature [41].

Figure 8(a) shows the Stokes shift at various QD concentrations, indicating a decrease in Stokes shift as a function of QD concentration. The Stokes shift is obtained by calculating the energy difference between the threshold energy of the absorption spectrum and the emission energy of PL. Combined with the results in Fig. 7(b), a decrease in the Stokes shift corresponds to a decrease (increase) in exciton delocalization (localization). From an earlier study, the Stokes shift is found to decrease with an increase of the emission energy in (In, Ga)N epilayers, which corresponds

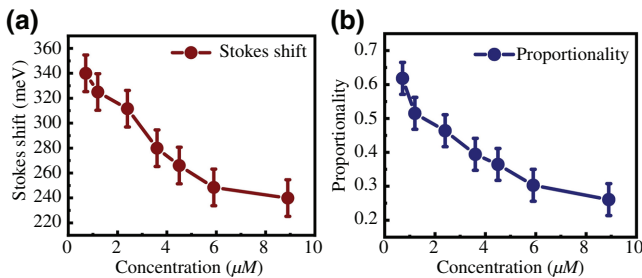


FIG. 8. (a) Stokes shift and (b) calculated coefficient of proportionality of the amino-functionalized MoS₂ QDs at various QD concentrations.

to a decrease in exciton localization [42]. The result for our QDs is thus in good agreement with studies on (In, Ga)N epilayers. Also, the Stokes shift can be a rough indicator of sample quality in 2D semiconductors as well [18]. Considering the topographical theory of the exciton spectra, the coefficient of proportionality between the Stokes shift and exciton absorption line width is demonstrated to be about 0.553 [18]. In our case, the Stokes shift (the FWHM of absorption) is about 340 meV (550 meV) at the lowest QD concentration (712 nM). Thus, the coefficient of proportionality at the lowest QD concentration is about 0.61, which is comparable with the topographical theory of exciton spectra (0.553). However, the coefficient of proportionality decreases to about 0.27 as the QD concentration increases to 8.9 μM, as shown in Fig. 8(b). We deduce that the decrease in proportionality is due to the presence of Davydov splitting, which broadens the peak in the absorption spectrum and misrepresents its FWHM.

To gain a better understanding of exciton delocalization in amino-functionalized MoS₂ QDs, we investigate the behavior of DETA concentration on the Davydov splitting. Figure 9 shows the PLE spectra of amino-functionalized MoS₂ QDs of different DETA concentrations under the chosen QD concentrations of 712 nM, 2.4 μM, 4.5 μM, and 8.9 μM. Other information regarding absorption, exciton energy, Davydov splitting, and exciton delocalization length of the amino-functionalized MoS₂ QDs in varying DETA concentrations are presented in Figs. S1–S3 within the Supplemental Material [43]. It is shown in Fig. 9(a) that the PLE exciton peaks found at the lowest QD concentrations do not exhibit Davydov splitting at all. Spectral broadening is only shown toward the high energy side. On

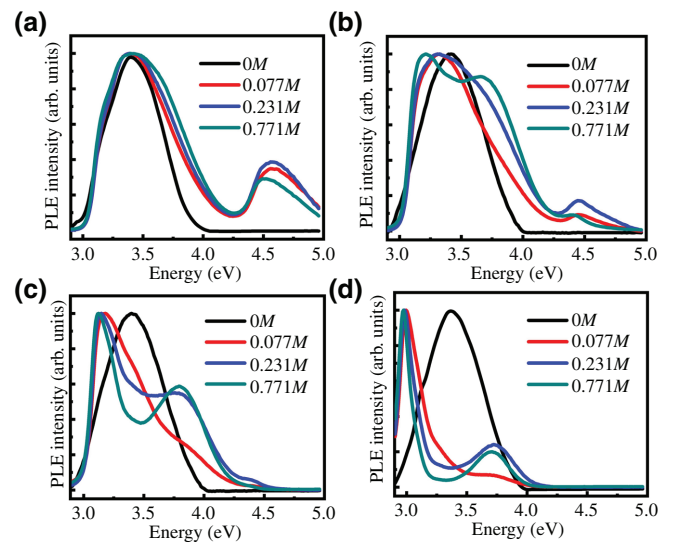


FIG. 9. PLE spectra of the exciton peak in amino-functionalized MoS₂ QDs as a function of DETA concentration at different QD concentrations of (a) 712 nM, (b) 2.4 μM, (c) 4.5 μM, and (d) 8.9 μM.

the other hand, as shown in Figs. 9(b)–9(d), the single exciton peak in PLE is split into two Davydov components and produces a pronounced spectral narrowing when there is a higher DETA concentration. Also, the splitting magnitude increases evidently as the DETA concentration increases from 0.077 to 0.771M. This indicates that the DETA concentration of amino-functionalized MoS₂ QDs plays an important role in the formation of Davydov splitting.

Here, we try to explain the influence of DETA concentration on exciton delocalization of the amino-functionalized MoS₂ QDs. Without DETA treatment, the pristine MoS₂ QDs attract each other through weak van der Waals force when they are nearby. This leads to a weak J-type aggregate, which corresponds to and explains the experimental result for the pristine MoS₂ QDs. However, surface-ligand functionalization on MoS₂ monolayers can produce the intrinsic dipole of the ligand itself and induce a dipole at the ligand-MoS₂ interface [44]. When DETA begins to be introduced into the MoS₂ QD (DETA concentration = 0.077M), the amino group from DETA can bind to MoS₂ QDs through sulfur vacancies and induce charge transfer, which causes *p*-type doping of MoS₂ QDs and creates a permanent dipole on the QD surface [45]. Therefore, the coupling in QDs would be enhanced because hydrogen bonds can be formed between amino groups, as described in Fig. 10(a). Furthermore, exchange narrowing of the exciton peak also appears due to the strong J-type aggregates. Finally, when the DETA concentration is increased further (0.231–0.771M), it gives the amino groups more opportunities to connect in different directions. When the transition dipoles of QDs have

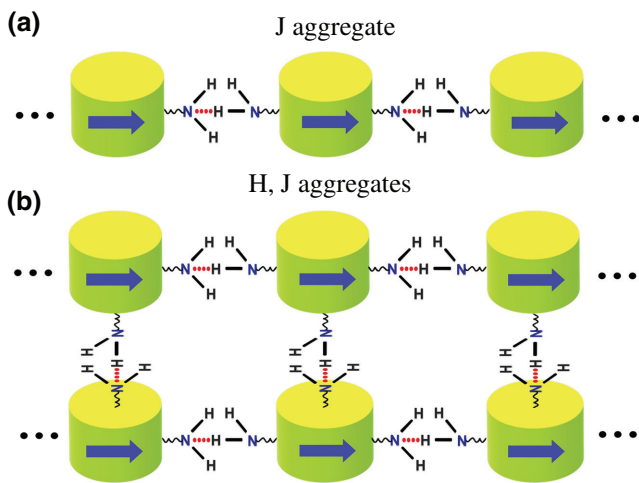


FIG. 10. Schematic representation of the transition dipole coupling for (a) J-type aggregates (head-to-tail stacking), and (b) the combination of H-type (parallel stacking) and J-type aggregates in amine-functionalized MoS₂ QDs. Blue arrow represents the transition dipole moment of MoS₂ QDs. Meanwhile, the amine group (on MoS₂ QDs) can bind to adjacent amine groups via hydrogen bonding (red dotted line).

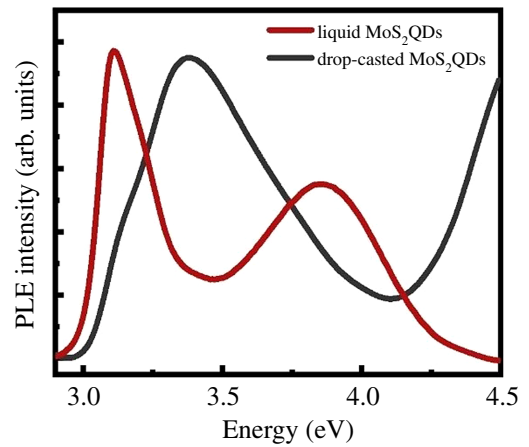


FIG. 11. PLE spectra of amine-functionalized MoS₂ QDs (QD concentration = 3.6 μ M and DETA concentration = 0.463M) in the liquid (red) and solid state (black).

the chance to be oriented parallel, the exciton energy shifts towards the high-energy side, indicating an H-type aggregate, which causes the blueshifted peaks. The amino-functionalized MoS₂ QDs develop head-to-tail and parallel stacking when combined with J-type and H-type aggregates [Fig. 10(b)]. Thus, Davydov splitting of the exciton peak in QDs is generated, as shown in Figs. 9(c) and 9(d). This explains the variation of exciton peaks in the amino-functionalized MoS₂ QDs by changing the DETA concentration from 0.231 to 0.771M. Considering the above results, the DETA concentration can be used to control the degree of exciton delocalization in the amino-functionalized MoS₂ QDs.

Recently, the alignment of the J aggregates of a uracil-functionalized BODIPY (boron-dipyrromethene) was implemented in a solid thin film [46]. It is thus desirable to investigate the effect of polarization on the Davydov splitting in the solid phase. Figure 11 shows the PLE spectra of amine-functionalized MoS₂ QDs in the liquid (red) and solid (black) states. The two Davydov components observed originally in the liquid state disappear after the QDs are cast on the glass substrate. The disappearance of Davydov splitting can be associated with changes in the environmental dielectrics. In TMD materials, the strength and form of excitons are very sensitive to the surrounding dielectrics [47]. Therefore, the variance in the screening effect from the dielectrics in the substrate (glass) greatly influences coulombic interactions in the solid-state MoS₂ QDs. This leads to a reduced excitonic interaction and, hence, to the disappearance of Davydov splitting.

IV. CONCLUSION

In this study, exciton delocalization in amino-functionalized MoS₂ QD aggregates is investigated by using

absorption and PLE spectra. Compared with the absorption spectra, the PLE spectra are found to be more sensitive for detecting the exciton transitions with radiative recombination in QD aggregates. A giant Davydov splitting as large as 850 meV and an exchange narrowing equivalent to a delocalization length occurring over several tens of QDs are observed at room temperature. The dependence of exciton delocalization in the amino-functionalized MoS₂ QDs on the DETA concentration is also investigated. Also, the stacking of QDs exhibits strong J-type aggregates for amino-functionalized MoS₂ QDs. For higher DETA concentrations (0.231–0.771M), a Davydov splitting of exciton peaks appears due to the head-to-tail and parallel stacking of QDs. Our results not only show that surface functional groups can play a decisive role in the generation of exciton coupling in 2D QD aggregates, but also provide a feasible manner to manipulate the coupling strength. This demonstration of exciton delocalization in inorganic semiconductors is expected to pave the way for the discovery of many interesting physical phenomena in different electronic and optical devices.

ACKNOWLEDGMENTS

This project is supported by the Ministry of Science and Technology in Taiwan under Grant No. MOST 109-2112-M-033-006-MY3.

The authors declare no conflicts of interest.

-
- [1] C. Kaufmann, W. Kim, A. Nowak-Król, Y. Hong, D. Kim, and F. Würthner, Ultrafast exciton delocalization, localization, and excimer formation dynamics in a highly defined perylene bisimide quadruple π -stack, *J. Am. Chem. Soc.* **140**, 4253 (2018).
- [2] B. Kriete, J. Lüttig, T. Kunsel, P. Malý, T. L. C. Jansen, J. Knoester, T. Brixner, and M. S. Pshenichnikov, Interplay between structural hierarchy and exciton diffusion in artificial light harvesting, *Nat. Commun.* **10**, 4615 (2019).
- [3] B. L. Cannon, D. L. Kellis, L. K. Patten, P. H. Davis, J. Lee, E. Graugnard, B. Yurke, and W. B. Knowlton, Coherent exciton delocalization in a Two-state DNA-templated Dye aggregate system, *J. Phys. Chem. A* **121**, 6905 (2017).
- [4] W. Liang, S. He, and J. Fang, Self-Assembly of J-aggregate nanotubes and their applications for sensing dopamine, *Langmuir* **30**, 805 (2014).
- [5] F. Fassioli, R. Dinshaw, P. C. Arpin, and G. D. Scholes, Photosynthetic light harvesting: Excitons and coherence, *J. R. Soc. Interface* **11**, 20130901 (2014).
- [6] D. Lubert-Perquel, E. Salvadori, M. Dyson, P. N. Stavrinou, R. Montis, H. Nagashima, Y. Kobori, S. Heutz, and C. W. M. Kay, Identifying triplet pathways in dilute pentacene films, *Nat. Commun.* **9**, 4222 (2018).
- [7] D. Abramavicius, B. Palmieri, D. V. Voronine, F. Šanda, and S. Mukamel, Coherent multidimensional optical spectroscopy of excitons in molecular aggregates; quasiparticle versus supermolecule perspectives, *Chem. Rev.* **109**, 2350 (2009).
- [8] B. S. Basel, C. Hetzer, J. Zirzmeier, D. Thiel, R. Guldi, F. Hampel, A. Kahnt, T. Clark, D. M. Guldi, and R. R. Tykwinski, Davydov splitting and singlet fission in excitonically coupled pentacene dimers, *Chem. Sci.* **10**, 3854 (2019).
- [9] J. Han, H. Zhang, and D. Abramavicius, Exchange narrowing and exciton delocalization in disordered J aggregates: Simulated peak shapes in the Two dimensional spectra, *J. Chem. Phys.* **139**, 034313 (2013).
- [10] J. Roden and A. Eisfeld, Anomalous strong exchange narrowing in excitonic systems, *J. Chem. Phys.* **134**, 34901 (2011).
- [11] A. Liess, A. Lv, A. Arjona-Esteban, D. Bialas, A.-M. Krause, V. Stepanenko, M. Stolte, and F. Würthner, Exciton coupling of merocyanine dyes from H- to J-type in the solid state by crystal engineering, *Nano Lett.* **17**, 1719 (2017).
- [12] B.-K. An, S.-K. Kwon, S.-D. Jung, and S. Y. Park, Enhanced emission and Its switching in fluorescent organic nanoparticles, *J. Am. Chem. Soc.* **124**, 14410 (2002).
- [13] D. H. Arias, K. W. Stone, S. M. Vlaming, B. J. Walker, M. G. Bawendi, R. J. Silbey, V. Bulović, and K. A. Nelson, Thermally-limited exciton delocalization in superradiant molecular aggregates, *J. Phys. Chem. B* **117**, 4553 (2013).
- [14] N. Kometani, H. Nakajima, K. Asami, Y. Yonezawa, and O. Kajimoto, Luminescence properties of the mixed J-aggregate of two kinds of cyanine dyes in layer-by-layer alternate assemblies, *J. Phys. Chem. B* **104**, 9630 (2000).
- [15] B. L. Cannon, L. K. Patten, D. L. Kellis, P. H. Davis, J. Lee, E. Graugnard, B. Yurke, and W. B. Knowlton, Large davydov splitting and strong fluorescence suppression: An investigation of exciton delocalization in DNA-templated holliday junction Dye aggregates, *J. Phys. Chem. A* **122**, 2086 (2018).
- [16] K. Broch, J. Dieterle, F. Branchi, N. J. Hestand, Y. Olivier, H. Tamura, C. Cruz, V. M. Nichols, A. Hinderhofer, D. Beljonne, F. C. Spano, G. Cerullo, C. J. Bardeen, and F. Schreiber, Robust singlet fission in pentacene thin films with tuned charge transfer interactions, *Nat. Commun.* **9**, 954 (2018).
- [17] M. Muccini, M. Schneider, C. Taliani, M. Sokolowski, E. Umbach, D. Beljonne, J. Cornil, and J. L. Brédas, Effect of wave-function delocalization on the exciton splitting in organic conjugated materials, *Phys. Rev. B* **62**, 6296 (2000).
- [18] F. Yang, M. Wilkinson, E. J. Austin, and K. P. O'Donnell, Origin of the Stokes Shift: A Geometrical Model of Exciton Spectra in 2D Semiconductors, *Phys. Rev. Lett.* **70**, 323 (1993).
- [19] Y. Narukawa, Y. Kawakami, S. Fujita, S. Fujita, and S. Nakamura, Recombination dynamics of localized excitons in In_{0.20}Ga_{0.80}N-In_{0.05}Ga_{0.95}N multiple quantum wells, *Phys. Rev. B* **55**, R1938 (1997).
- [20] Y.-H. Cho, G. H. Gainer, A. J. Fischer, J. J. Song, S. Keller, U. K. Mishra, and S. P. DenBaars, "S-Shaped" temperature-dependent emission shift and carrier dynamics in InGaN/GaN multiple quantum wells, *Appl. Phys. Lett.* **73**, 1370 (1998).
- [21] K. Yao, A. Yan, S. Kahn, A. Suslu, Y. Liang, E. S. Barnard, S. Tongay, A. Zettl, N. J. Borys, and P. J. Schuck, Optically

- Discriminating Carrier-Induced Quasiparticle Band gap and Exciton Energy Renormalization in Monolayer MoS₂, *Phys. Rev. Lett.* **119**, 087401 (2017).
- [22] T. N. Lin, S. R. M. Santiago, S. P. Caigas, C. T. Yuan, T. Y. Lin, J. L. Shen, and Y. F. Chen, Many-Body effects in doped WS₂ monolayer quantum disks at room temperature, *Npj 2D Mater. Appl.* **3**, 46 (2019).
- [23] B. Z. Tang, Optoelectronic applications of functional materials with aggregation-induced emissions (conference presentation), in Proc. SPIE 10361, 1036106 (2017).
- [24] J. Xiao, M. Zhao, Y. Wang, and X. Zhang, Excitons in atomically thin 2D semiconductors and their applications, *Nanophotonics* **6**, 1309 (2017).
- [25] H. Zhang, S. B. Lu, J. Zheng, J. Du, S. C. Wen, D. Y. Tang, and K. P. Loh, Molybdenum disulfide (MoS₂) as a broadband saturable absorber for ultra-fast photonics, *Opt. Express* **22**, 7249 (2014).
- [26] A. Autere, H. Jussila, Y. Dai, Y. Wang, H. Lipsanen, and Z. Sun, Nonlinear optics with 2D layered materials, *Adv. Mater.* **30**, 1705963 (2018).
- [27] R. Kaindl, B. C. Bayer, R. Resel, T. Müller, V. Skakalova, G. Habler, R. Abart, A. S. Cherevan, D. Eder, M. Blatter, F. Fischer, J. C. Meyer, D. K. Polyushkin, and W. Waldhauser, Growth, structure and stability of sputter-deposited MoS₂ thin films, *Beilstein J. Nanotechnol.* **8**, 1115 (2017).
- [28] B. Ni and X. Wang, Face the edges: Catalytic active sites of nanomaterials, *Adv. Sci.* **2**, 1500085 (2015).
- [29] R. Addou, L. Colombo, and R. M. Wallace, Surface defects on natural MoS₂, *ACS Appl. Mater. Interfaces* **7**, 11921 (2015).
- [30] M. Manuja, V. Sarath Krishnan, and G. Jose, Molybdenum disulphide nanoparticles synthesis using a low temperature hydrothermal method and characterization, *IOP Conf. Ser. Mater. Sci. Eng.* **360**, 12015 (2018).
- [31] G. Deokar, P. Vancsó, R. Arenal, F. Ravoux, J. Casanova-Cháfer, E. Llobet, A. Makarova, D. Vyalikh, C. Struzzi, P. Lambin, M. Jouiad, and J. F. Colomer, MoS₂-carbon nanotube hybrid material growth and Gas sensing, *Adv. Mater. Interfaces* **4**, 1700801 (2017).
- [32] L. Shen and N. Wang, Effect of nitrogen pressure on the structure of Cr-N, Ta-N, Mo-N, and W-N nanocrystals synthesized by Arc discharge, *J. Nanomater.* **2011**, 781935 (2011).
- [33] M. Fu, F. Ehrat, Y. Wang, K. Z. Milowska, C. Reckmeier, A. L. Rogach, J. K. Stolarczyk, A. S. Urban, and J. Feldmann, Carbon dots: A unique fluorescent cocktail of polycyclic aromatic hydrocarbons, *Nano Lett.* **15**, 6030 (2015).
- [34] M. Noh, T. Kim, H. Lee, C.-K. Kim, S.-W. Joo, and K. Lee, Fluorescence quenching caused by aggregation of water-soluble CdSe quantum dots, *Colloids Surfaces A Physicochem. Eng. Asp.* **359**, 39 (2010).
- [35] A. Yassar, G. Horowitz, P. Valat, V. Wintgens, M. Hmyene, F. Deloffre, P. Srivastava, P. Lang, and F. Garnier, Exciton coupling effects in the absorption and photoluminescence of sexithiophene derivatives, *J. Phys. Chem.* **99**, 9155 (1995).
- [36] J. E. Huheey, The electronegativity of multiply bonded groups, *J. Phys. Chem.* **70**, 2086 (1966).
- [37] M. Kasha, M. A. El-Bayoumi, and W. Rhodes, Excited states of nitrogen base-pairs and polynucleotides, *J. Chim. Phys.* **58**, 916 (1961).
- [38] A. J. Cadby, J. Partee, J. Shinar, S. J. Martin, C. W. Spangler, D. D. C. Bradley, and P. A. Lane, Optical studies of molecular aggregates: The photophysics of a thienylene vinylene oligomer, *Phys. Rev. B* **65**, 245202 (2002).
- [39] T. Cosby, Z. Vicars, E. U. Mapesa, K. Tsunashima, and J. Sangoro, Charge transport and dipolar relaxations in phosphonium-based ionic liquids, *J. Chem. Phys.* **147**, 234504 (2017).
- [40] L. D. Bakalis and J. Knoester, Pump-probe spectroscopy and the exciton delocalization length in molecular aggregates, *J. Phys. Chem. B* **103**, 6620 (1999).
- [41] G. Y. Guralchuk, A. V. Sorokin, I. K. Katrunov, S. L. Yefimova, A. N. Lebedenko, Y. V. Malyukin, and S. M. Yarmoluk, Specificity of cyanine dye L-21 aggregation in solutions with nucleic acids, *J. Fluoresc.* **17**, 370 (2007).
- [42] R. W. Martin, P. G. Middleton, K. P. O'Donnell, and W. Van Der Stricht, Exciton localization and the stokes' shift in InGaN epilayers, *Appl. Phys. Lett.* **74**, 263 (1999).
- [43] See the Supplemental Material at <http://link.aps.org/supplemental/10.1103/PhysRevApplied.15.024011> for calculations of the DETA and QD concentrations, as well as characterization and other supporting measurements in absorption, exciton energy, Davydov splitting, and exciton delocalization length of amino-functionalized inorganic MoS₂ quantum disks.
- [44] J. Pan, Z. Wang, Q. Chen, J. Hu, and J. Wang, Band structure engineering of monolayer MoS₂ by surface ligand and functionalization for enhanced photoelectrochemical hydrogen production activity, *Nanoscale* **6**, 13565 (2014).
- [45] E. Satheshkumar, A. Bandyopadhyay, M. B. Sreedhara, S. K. Pati, C. N. R. Rao, and M. Yoshimura, One-step simultaneous exfoliation and covalent functionalization of MoS₂ by amino acid induced solution processes, *ChemNanoMat* **3**, 172 (2017).
- [46] Y. Zhang, P. Liu, H. Pan, H. Dai, X. K. Ren, and Z. Chen, Alignment of supramolecular J-aggregates based on uracil-functionalized BODIPY dye for polarized photoluminescence, *Chem. Commun.* **56**, 12069 (2020).
- [47] Y. Lin, X. Ling, L. Yu, S. Huang, A. L. Hsu, Y. H. Lee, J. Kong, M. S. Dresselhaus, and T. Palacios, Dielectric screening of excitons and trions in single-layer MoS₂, *Nano Lett.* **14**, 5569 (2014).